

Supporting information

Electrochemical and Photoelectrochemical Water Splitting with CoO_x Catalyst Prepared by Flame Assisted Deposition

Fusheng Li,^{*†} Ziqi Zhao,[†] Hao Yang,^b Dinghua Zhou,^a Yilong Zhao,^a Yingzheng Li,^a
Wenlong Li,^a Xiujuan Wu,^a Peili Zhang^a and Licheng Sun^{*a, b}

a) State Key Laboratory of Fine Chemicals, Institute of Artificial Photosynthesis, DUT-KTH Joint Education and Research Centre on Molecular Devices, Institute for Energy Science and Technology, Dalian University of Technology, Dalian 116024, P. R. China

b) Department of Chemistry, School of Engineering Sciences in Chemistry, Biotechnology and Health, KTH Royal Institute of Technology, Stockholm 10044, Sweden.

fusheng@dlut.edu.cn

lichengs@kth.se

[†]These authors contributed equally to this work.

Experimental Section

Physical Characterization

The morphology of all films was characterized by field emission scanning electron microscopy (HITACHI UHR FE-SEM SU8220, operated at 5 and 10 KV) and the elemental mappings were obtained from energy dispersive X-ray (EDX) microanalysis (Oxford EDS Inca Energy Coater 300). High-resolution transmission electron microscopy (HR-TEM) and elemental mappings were obtained from the TF30 (Thermo Scientific) operating at an acceleration voltage of 300 kV. The crystal information was tested by X-Ray Diffraction (XRD D/Max-2400). The element valence state of films was analyzed by X-ray photoelectron spectroscopy (XPS, Thermo Fisher ESCALAB™ Xi⁺). The vibration and rotation of chemical bands were investigated by Micro-Raman spectra (Thermo Fisher DXR Microscope). The absorption spectra of photoanodes was taken by Solid UV-Visible (UV-vis) Spectrometer (Thermo Scientific Evolution 200).

Materials and Reagents

Potassium phosphate dibasic (K_2HPO_4 , 99%), potassium phosphate monobasic (KH_2PO_4 , 99.5%), sodium nitrate ($NaNO_3$, 99%), potassium hydroxide (KOH, 99%), hydrochloric acid (HCl, 37%), cobalt nitrate hexahydrate ($Co(NO_3)_2 \cdot 6H_2O$, 99.99%), ferric chloride hexahydrate ($FeCl_3 \cdot 6H_2O$, 99%) and sodium tetraborate decahydrate ($Na_2B_4O_7 \cdot 10H_2O$, 99.95%) were purchased from Aladdin[®] China. Dihydroxybis (ammonium

lactate) titanium (IV) (TALH, 50% w/w aq. soln) was purchased from Alfa Aesar. The high purity water ($18.2 \text{ M}\Omega\cdot\text{cm}^{-1}$) used in all tests was supplied by a Milli-Q system. Fluorine-doped tin oxide conductive glass (FTO, NGS 8Ω $10 \text{ mm}\times 25 \text{ mm}\times 1 \text{ mm}$), all the FTO substrates in all experiments were cleaned with deionized water, ethanol and acetone by ultrasonic cleaning machine for 20 min before used. All organic solvents were directly used without purification. Alcohol lamp and wick were all purchased in the local supplier.

Preparation of FAD-CoO_x/FTO

5.82 g of $\text{Co}(\text{NO}_3)_2\cdot 6\text{H}_2\text{O}$ (0.02 mol) was first dissolved in 200 mL of methanol, then the solution was transferred into an alcohol lamp. After igniting the lamp, in order to make the flame stable, the flame was covered by a quartz tube. A FTO glass was fixed by a clamp (the conductive side downward), which was horizontally moved on the flame (the 2 cm above the top of flame) for 1 min. After cooling down to room temperature, the resulting FAD-CoO_x/FTO electrode was then rinsed with deionized water and dried by airflow. The mechanism of FAD process can be interpreted as follows: methanol precursor cobalt nitrate produces cobalt nitrate vapor along with the combustion reaction and generated CoO_x was rapidly deposited on a cooler FTO substrate surface. And the reaction equation might meet with the following: $\text{Co}(\text{NO}_3)_2\cdot 6\text{H}_2\text{O} \rightarrow \text{CoO}_x + \text{NO}_x + \text{O}_2 + \text{H}_2\text{O}$.

Preparation of Co-Pi/FTO

The reference sample, benchmarked water oxidation catalyst cobalt phosphate (Co-Pi), was prepared according to literature.¹ Briefly, a three-electrode cell was used for the electro-deposition process with a FTO as the working electrode, a saturated Ag/AgCl as the reference electrode, and a platinum mesh as the counter electrode. The solution of 0.5 mM $\text{Co}(\text{NO}_3)_2 \cdot 6\text{H}_2\text{O}$ in 0.1 M pH 7 potassium phosphate buffer (KPi) was used as the electrolyte. A potentiostatic deposition process was carried out at 1.05 V vs Ag/AgCl with a charge of 20 mC/cm² passed through the FTO. The resulting Co-Pi/FTO electrode was rinsed with deionized water and dried by airflow.

Fabrication of TiO₂ Modified Hematite Films (TiO₂/Fe₂O₃)

The TiO₂/Fe₂O₃ film was prepared by a modified method from the literature report.^{2,3} Briefly, 169.98 g of NaNO₃ (2 mol) and 81.04 g of FeCl₃·6H₂O (0.3 mol) was dissolved in 1 L deionized water. The pH of this solution was adjusted to 1.5. The surface of cleaned FTO glass substrate was covered by Kapton tapes (3M) with an area of 1×1 cm² of the conductive side reserved. The FTO glass was immersed into 15 mL of above solution in a sealed glass vial. The reaction was placed in an oven at 95°C for 5 h, and a yellowish film formed on the FTO glass. After rinsing with water, the precursor film was sintered at 800°C for 10 min (ramping rate 15°C/min). The as-prepared Fe₂O₃ substrates were dipped in a TALH

solution (2.5 mM at pH 5.6) for 1 h. After rinsed with deionized water, the TALH treated Fe_2O_3 was calcined at 350 °C for 1 h (ramping rate 10°C/min), resulting in the TiO_2 modified hematite film ($\text{TiO}_2/\text{Fe}_2\text{O}_3$).

Preparation of Co-Pi/ $\text{TiO}_2/\text{Fe}_2\text{O}_3$

The deposition of Co-Pi on hematite was according to reference.⁴ The $\text{TiO}_2/\text{Fe}_2\text{O}_3$ prepared as above was used as working electrode, a Ag/AgCl as the reference electrode and a platinum mesh as the counter electrode in a three-electrode configuration. The electrolyte was 0.5 mM $\text{Co}(\text{NO}_3)_2$ in 0.1 M KPi buffer (pH 7). Potentiostatic deposition method was applied to obtain Co-Pi/ $\text{TiO}_2/\text{Fe}_2\text{O}_3$ photoanodes. The potential is set to 1.05 V vs Ag/AgCl. The deposition time was set as 1 min to match the flame assisted deposition time of our FAD- CoO_x catalyst.

Preparation of FAD- $\text{CoO}_x/\text{TiO}_2/\text{Fe}_2\text{O}_3$

The FAD- $\text{CoO}_x/\text{TiO}_2/\text{Fe}_2\text{O}_3$ electrode was prepared by the same method to FAD- CoO_x/FTO electrode.

Electrochemical Measurements

All electrochemical tests were performed on a CHI 660e electrochemical workstation in a three-electrode system with a platinum mesh as the counter electrode, a Ag/AgCl as the reference electrode and the CoO_x/FTO as the working electrode. A 1.0 M borate buffer solution (KB, pH 9.2) was used as the electrolyte. Unless specified, all cyclic

voltammetry (CV) and linear scan voltammetry (LSV) were tested with a scan rate of 50 mV sec⁻¹, the equation of $E_{NHE} = E_{Ag/AgCl} + 0.195$ was used to convert the potentials into normal hydrogen electrode (NHE) scale.

Turn Over Frequency (TOF) Calculation

The TOF of the electrochemical activity Co for FAD-CoO_x was calculated by **eqn. S1**,⁵

$$TOF = \frac{JA}{4F\Gamma A} \quad \text{eqn. S1}$$

Where **J** is water oxidation current density (A cm⁻²) corresponding in CV curve with a lower scan rate, **A** is the surface area in measurement (cm²), **F** is Faradaic constant (96485 C mol⁻¹). **Γ** is the amount of electrochemical activity Co (mol cm⁻²), which can be calculated from **eqn. S2**, there is a linear correlation between the slope and **Γ**, when plotting the peak current of Co vs different scan rates.

$$i_p = \frac{n^2 F^2 \nu A \Gamma}{4RT} \quad \text{eqn. S2}$$

Where **i_p** is peak current of the electrochemical activity Co (here is redox peak of Co), **n** is number of transfer electrons (for this system, **n** = 1), **ν** is scan rate (V s⁻¹), **R** is ideal gas constant (8.314 JK⁻¹mol⁻¹) and **T** is temperature (298 K).⁶

Photo-electrochemical Measurements

All photoelectrochemical measurements were carried out on a CHI

760e electrochemical workstation. The catalytic performance of photoanodes was evaluated in a typical three-electrode configuration with the prepared photoanodes ($1 \times 1 \text{ cm}^2$) as working electrode, a platinum mesh as the counter electrode and a Hg/HgO (1 M KOH) as the reference electrode in a 1.0 M KOH solution as electrolyte (pH = 13.6). The simulated solar illumination was obtained by a 300 W Xenon arc lamp (EXCELITAS, PE300BFA) equipped with an AM 1.5G filter. The irradiation intensity of the light was adjusted to 100 mW cm^{-2} by a Newport OMM-6810B photometer (OMH-6742B, Silicon detector, 350-1100nm). Photocurrent-potential curves were recorded by LSV with a scan rate of 10 mV sec^{-1} . The recorded potential was converted into reversible hydrogen electrode (RHE) according to equation $E_{RHE} = E_{Hg/HgO} + 0.098 + 0.059 \text{ pH}$.

The incident photon to current efficiency (IPCE)

IPCE was measured by using the 300 W Xenon arc lamp equipped with a monochromator. In short, the photocurrent density (J_{light}) and dark current density (J_{dark}) of photoanode were measured at an applied potential of 1.23 V vs RHE with a controlled active area ($0.5 \times 0.5 \text{ cm}^2$). The intensity of each monochromatic light (P_{λ}) at given wavelength (λ) was recorded by a photometer (Newport OMM-6810B). According to **eqn. S3**, the IPCE values can be calculated.

$$IPCE(\%) = \frac{1240 \times (J_{light} - J_{dark})}{\lambda \times P_{\lambda}} \times 100\% \quad \text{eqn. S3}$$

The applied bias photon-to-current efficiency (ABPE)

ABPE was obtained by converting the LSV curves from **Fig. 3a** in the main text according to **eqn. S4**.

$$ABPE(\%) = \frac{(1.23 - V_{RHE}) \times (J_{light} - J_{dark})}{P_{light}} \times 100\% \quad \text{eqn. S4}$$

The electrochemical impedance spectroscopy (EIS)

Nyquist plots were performed with a bias potential at 0.9 V vs RHE under 100 mW cm⁻² light illumination. The frequency range was set between 100 kHz to 0.1 Hz with an amplitude frequency of 10 mV.

Intensity Modulated Photocurrent Spectroscopy (IMPS)

The IMPS spectrum of photoanode was carried out a Zahner photoelectrochemical workstation (CIMPS-2). A white light-emitting diode (LED) with light intensity of 100 mW cm⁻² was used as the light source. The ac current input of LED was derived from a 10% superimposition of sinusoidal modulation. The setup of IMPS spectrum was same as photoelectrochemical measurements. All IMPS data was recorded with a frequency ranging from 100 mHz to 100 kHz at different applied bias 0.8, 0.9, 0.95, 1.0, 1.05, 1.1 V vs RHE, respectively.

Measurements of Faradaic efficiency:

The amount of oxygen evolution from the photoelectrochemical reaction was determined by gas chromatography (Techcomp GC 7890T, Ar carrier gas, Thermo Conductivity Detector). Galvanostatic method (1 mA cm⁻²) and potentiostatic method (at 1.23 V vs RHE) were used to electrochemical and photoelectrochemical measurements, respectively. The theoretical O₂ evolution can be calculated by the amount of charge passed through electrodes.

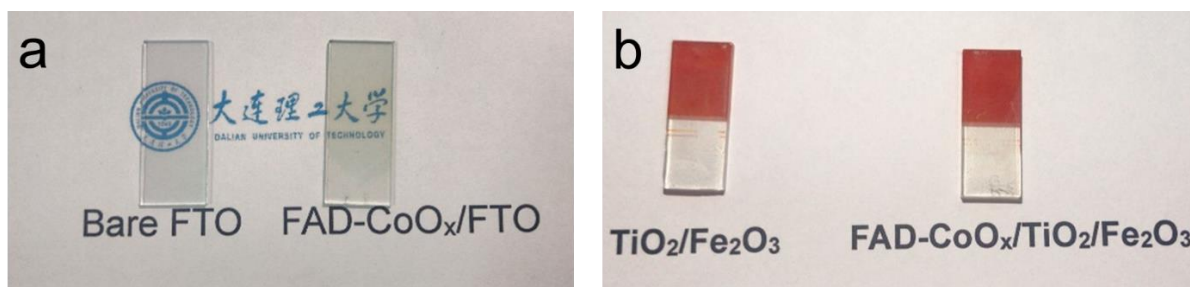


Figure S1. Optical photographs of (a) FAD-CoO_x/FTO and FTO, (b) FAD-CoO_x/TiO₂/Fe₂O₃ and TiO₂/Fe₂O₃.

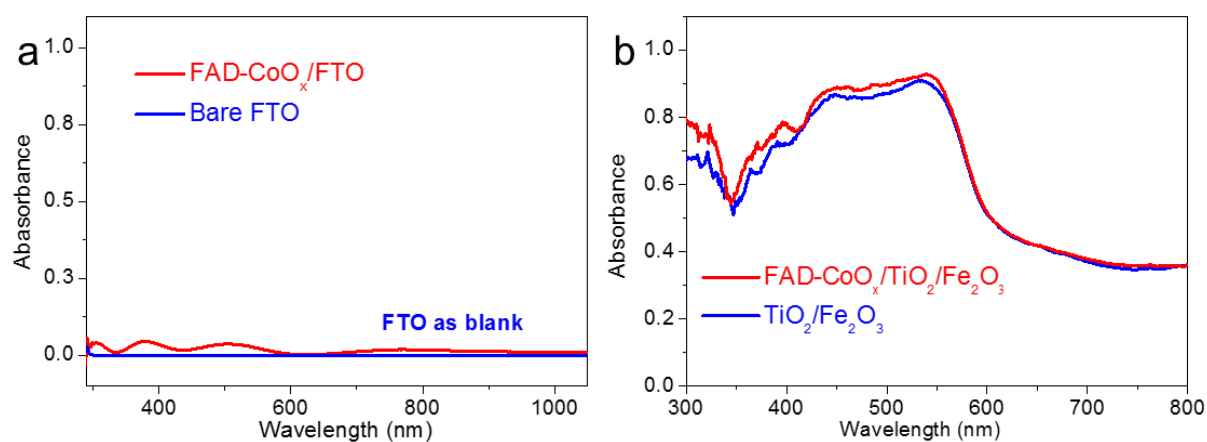


Figure S2. UV-vis spectra of (a) FAD-CoO_x/FTO and FTO, (b) FAD-CoO_x/TiO₂/Fe₂O₃ and TiO₂/Fe₂O₃.

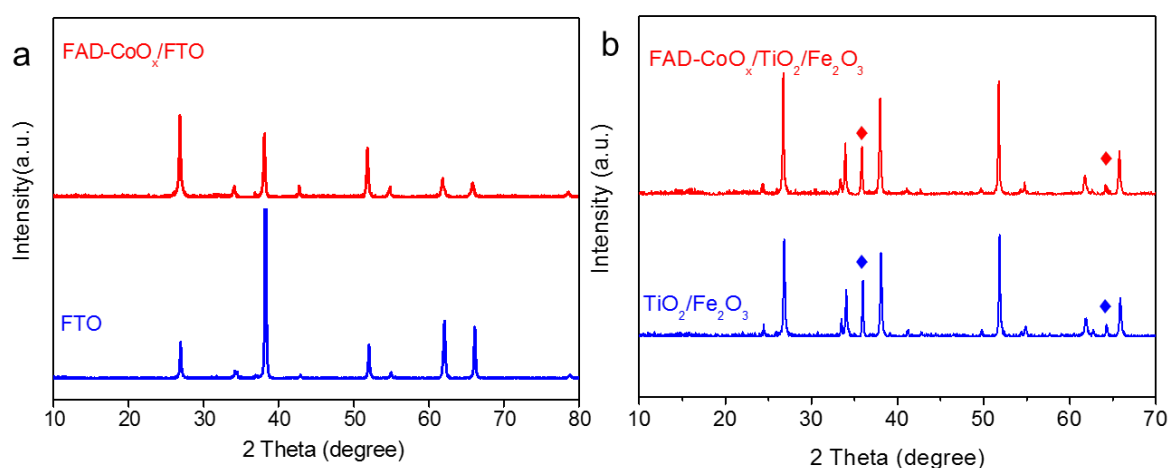


Figure S3. XRD spectra of the (a) FAD-CoO_x/FTO and FTO, (b) FAD-CoO_x/TiO₂/Fe₂O₃ and TiO₂/Fe₂O₃.

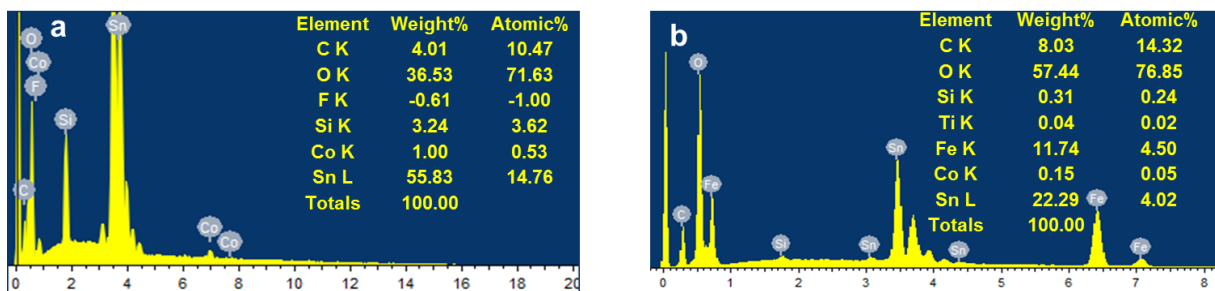


Figure S4. Energy dispersive X-ray spectra (EDS) of (a) FAD-CoO_x/FTO and (b) FAD-CoO_x/TiO₂/Fe₂O₃.

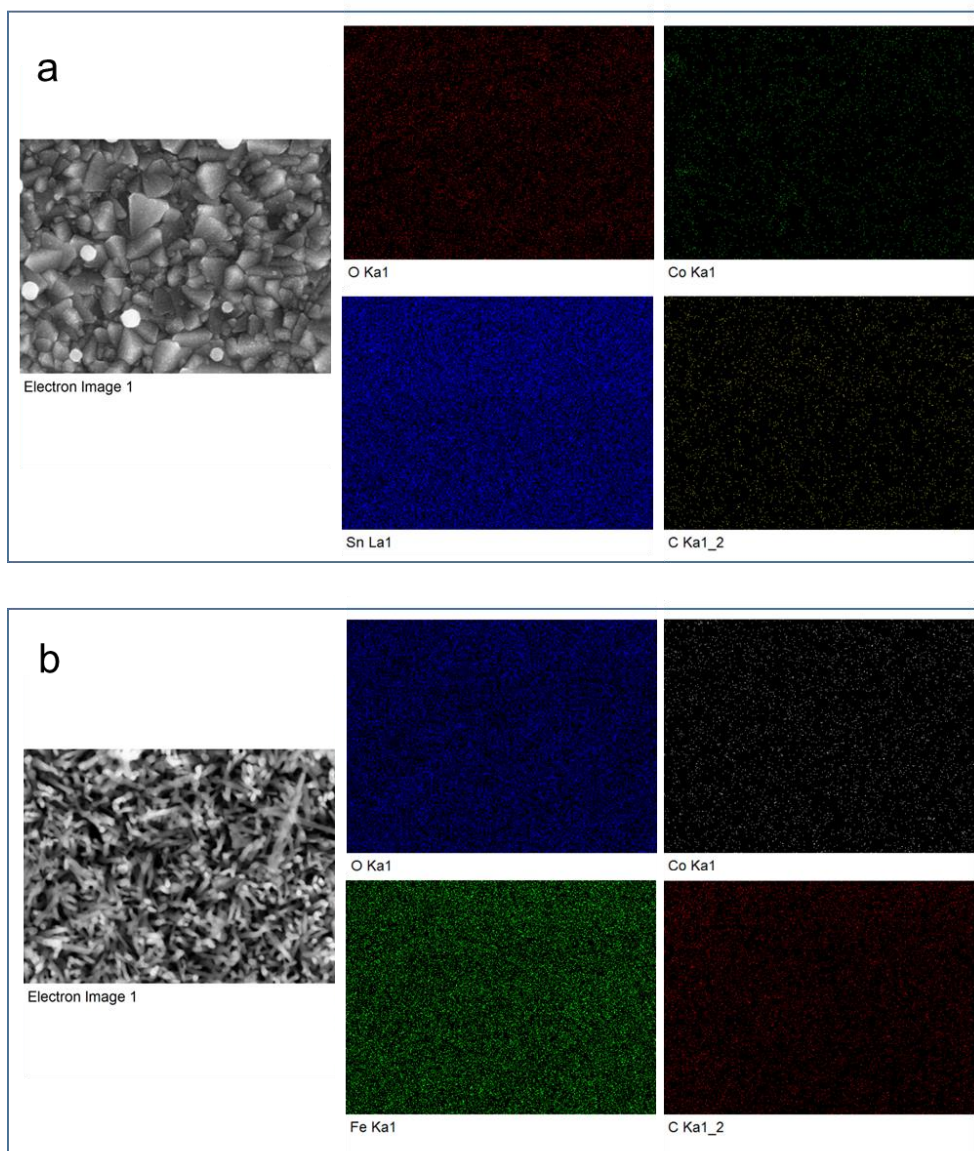


Figure S5. EDS element-mapping images of (a) FAD-CoO_x/FTO and (b) FAD-CoO_x/TiO₂/Fe₂O₃.

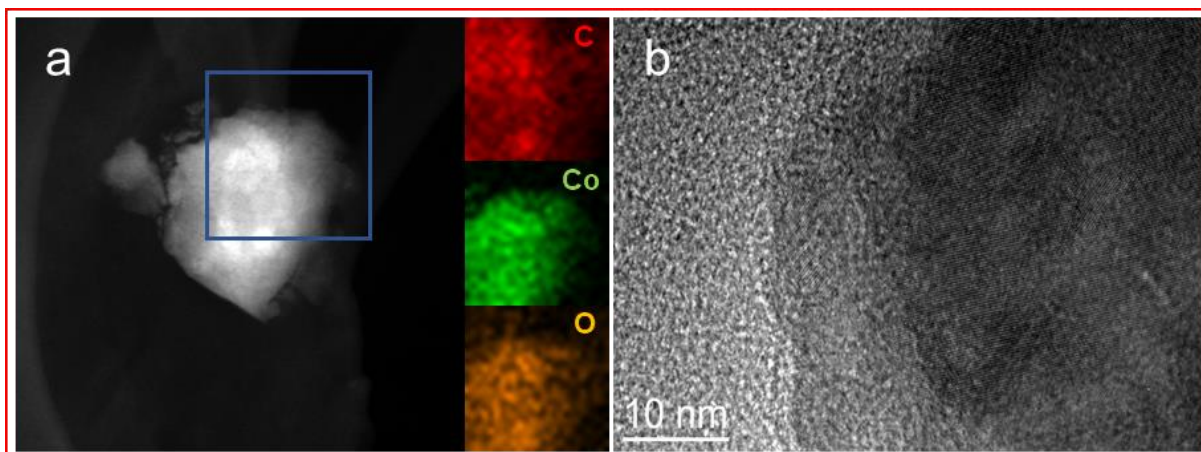


Figure S6. (a) Dark field scanning TEM image of FAD-CoO_x on FTO electrode and corresponding elemental mappings for select region. (b) HRTEM image of the FAD-CoO_x on FTO electrodes.

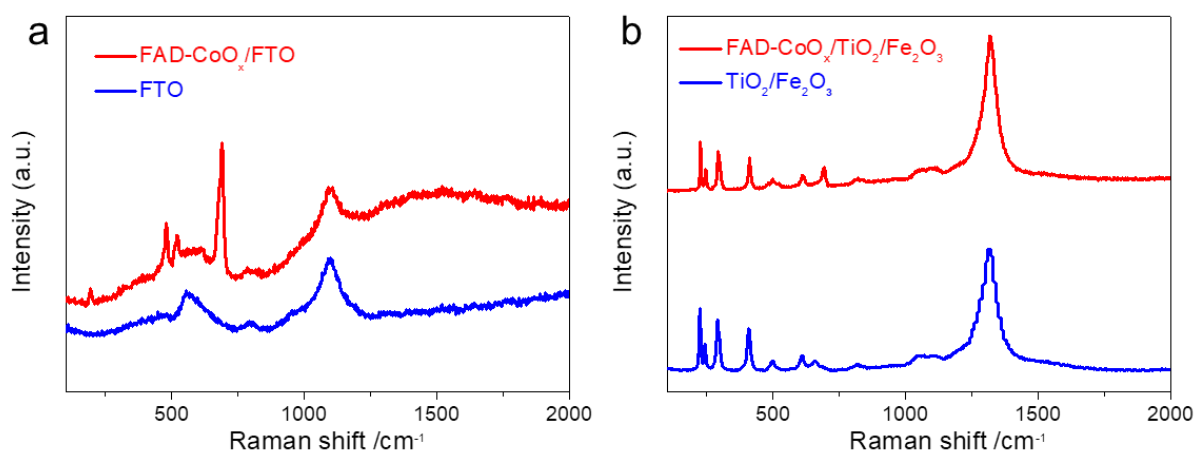


Figure S7. Raman spectra of (a) FAD-CoO_x/FTO and FTO, (b) FAD-CoO_x/TiO₂/Fe₂O₃ and TiO₂/Fe₂O₃.

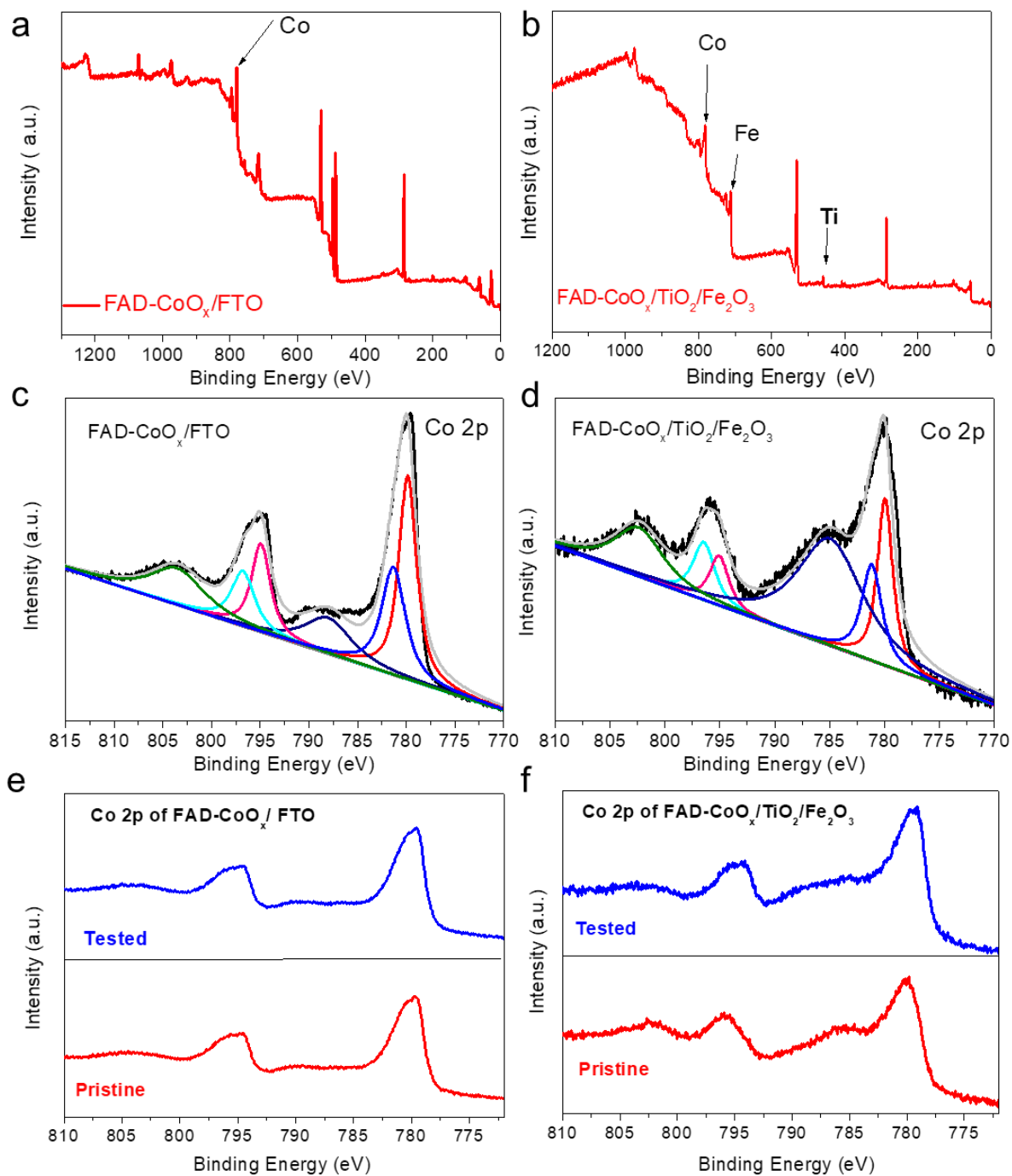


Figure S8. XPS survey spectra of (a) FAD-CoO_x/FTO and (b) FAD-CoO_x/TiO₂/Fe₂O₃. And the high-resolution XPS spectra of Co 2p for (c) FAD-CoO_x/FTO and (d) FAD-CoO_x/TiO₂/Fe₂O₃. The comparison of XPS spectra of Co 2p before and after OER measurements: (e) FAD-CoO_x/FTO and (f) FAD-CoO_x/TiO₂/Fe₂O₃.

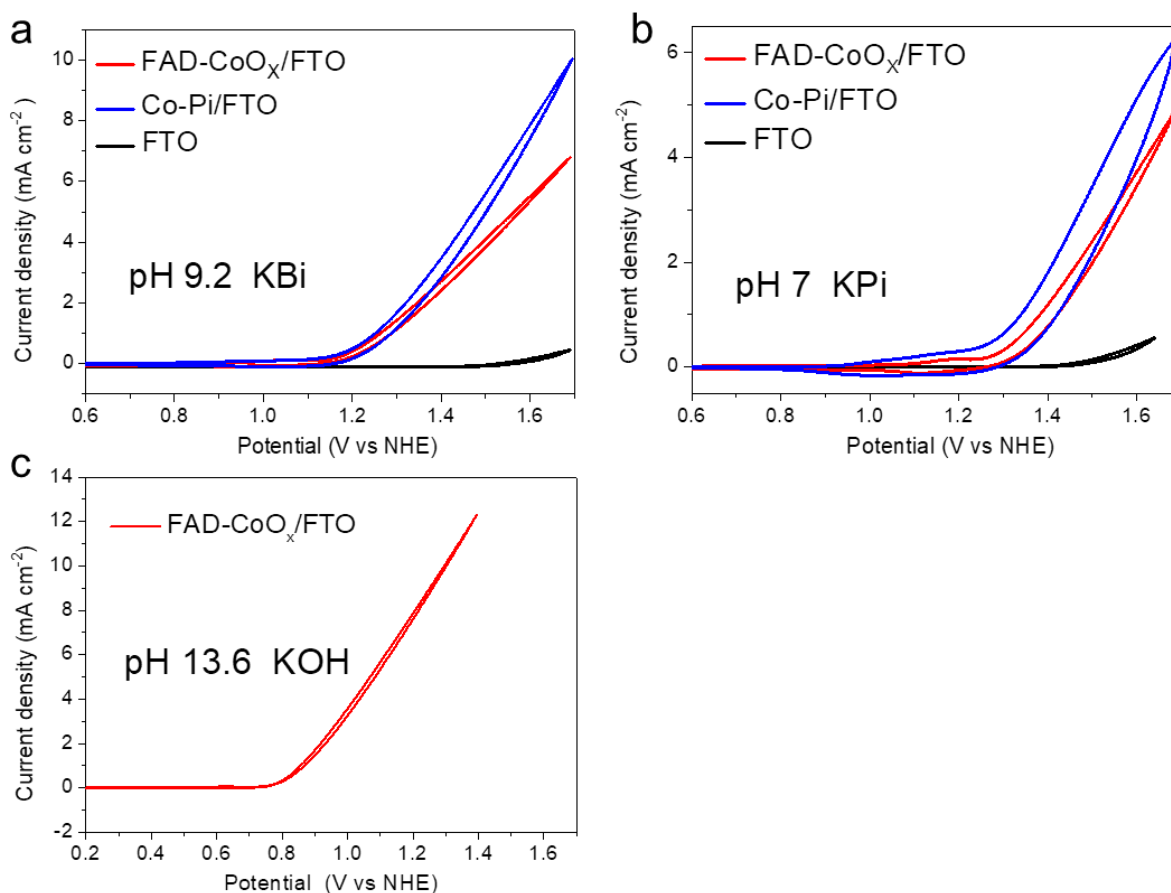


Figure S9. (a) The comparison CV measurements of FAD-CoO_x/FTO, Co-Pi/FTO and bare FTO electrode in 1.0 M borate buffer (pH 9.2) and (b) 0.1 M potassium phosphate (pH 7) at a scan rate of 50 mV s⁻¹ with no *iR* compensation. (c) The CV measurement of FAD-CoO_x/FTO in 1.0 M KOH (pH 13.6) at a scan rate of 50 mV s⁻¹ with no *iR* compensation.

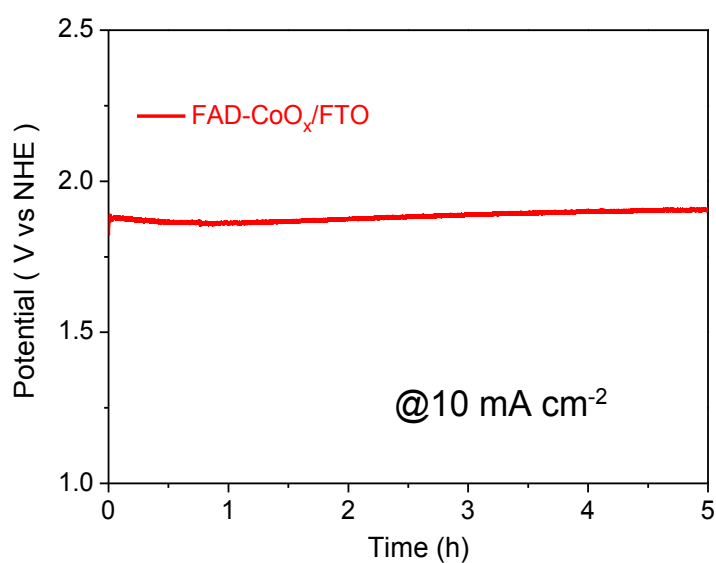


Figure S10. Chronopotentiometric measurements of FAD-CoO_x/FTO at $j = 10 \text{ mA cm}^{-2}$ in 1.0 M borate buffer (pH 9.2) for 5h with no *iR* compensation.

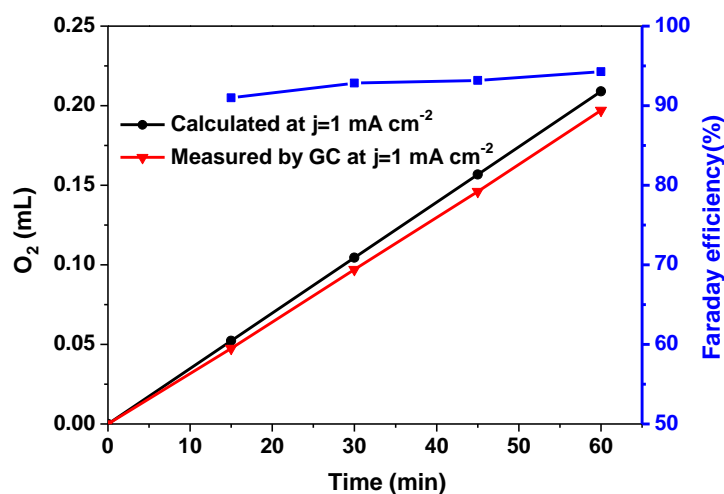


Figure S11. Faradic efficiency of FAD-CoO_x/FTO system for OER in 1.0 M borate buffer (pH 9.2) under the galvanostatic method of 1 mA cm⁻². The Faradic efficiency was calculated from practical and theoretical oxygen evolution.

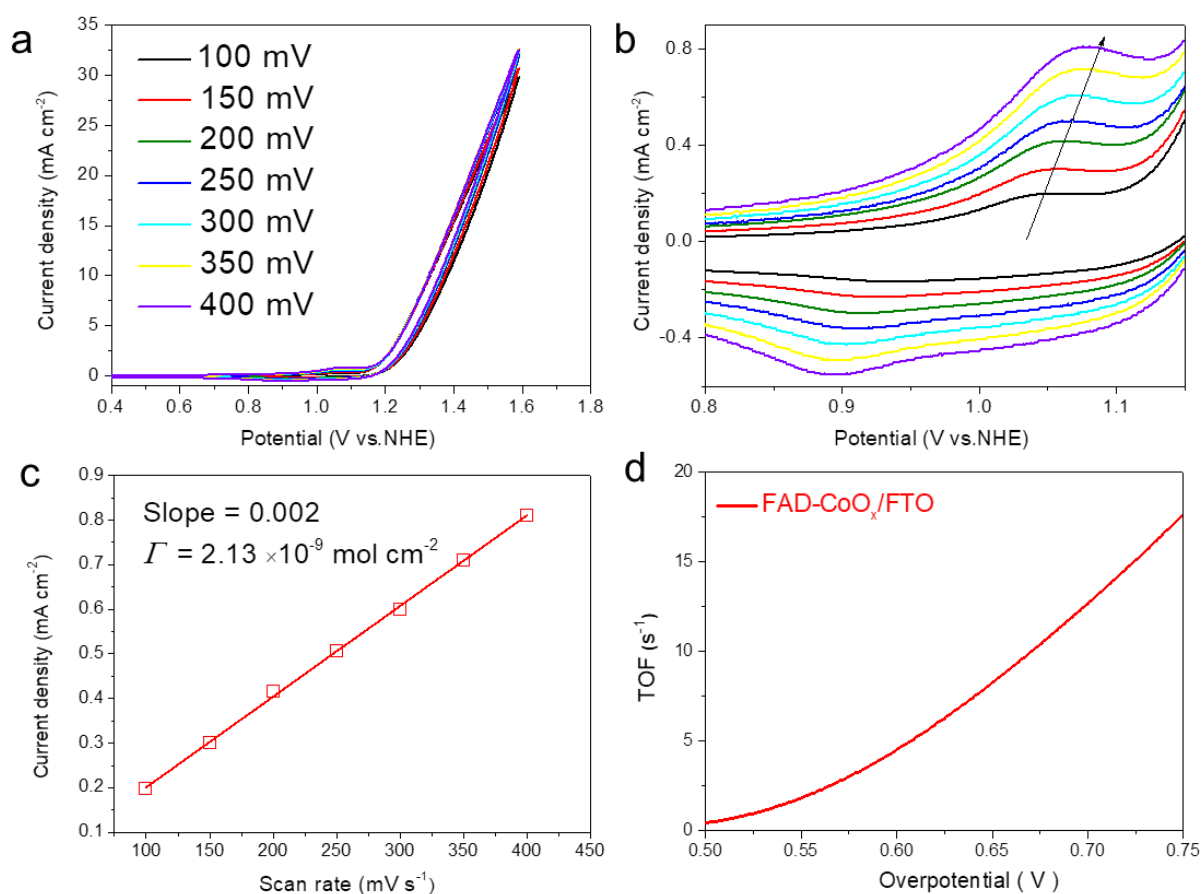


Figure S12. (a) CV curves of FAD-CoO_x/FTO electrode under various scan rates (100 ~ 400 mV s⁻¹) in a borate buffer (pH 9.2) and (b) the corresponding magnified area. (c) Linear fitting between the redox peak current density and scan rate. (d) the calculate TOF according to the data from **Fig. 2a** in the main text.

Table S1. Water oxidation performance of recently published catalysts immobilized on conducting glass substrates (FTO or ITO).

| Catalyst | immobilization method | Loading (nmol cm ⁻²) | Electrolyte | η (mV at $j = 1 \text{ mA cm}^{-2}$) | TOF (h ⁻¹) | Ref. |
|---|----------------------------------|----------------------------------|---------------------------|--|--|------------------|
| FAD-CoO_x | flame-assisted deposition | 2.13 | 1.0 M KBi (pH 9.2) | 490 | 4032 (1.12 s⁻¹) (530 mV) | This work |
| Fe-based | electrodeposition | 10.2 | 0.1 M Pi (pH 7) | 480 | 756 (530 mV) | 7 |
| MnO _x | electrodeposition | 80 | 0.1 M Pi (pH 7) | 590 | 36 (530 mV) | 8 |
| Co-Pi | electrodeposition | 100 | 0.1 M Pi (pH 7) | 550 | 61.2 (530 mV) | 9,10 |
| Mn ₃ (PO ₄) ₂ | precipitation | 611 | 0.5 M Pi (pH 7) | 680 | 4.4 (680 mV) | 11 |
| LiMnP ₂ O ₇ | solid-state synthesis | 1059 | 0.5 M Pi (pH 7) | 680 | 4.2 (680 mV) | 12 |
| NiO _x -en | electrodeposition | 270 | 0.1 M NaBi (pH 9.2) | 510 | 54 (610 mV) | 13 |
| Cu-Bi | electrodeposition | N/A | 0.2 M Bi (pH 9) | 576 | N/A | 14 |

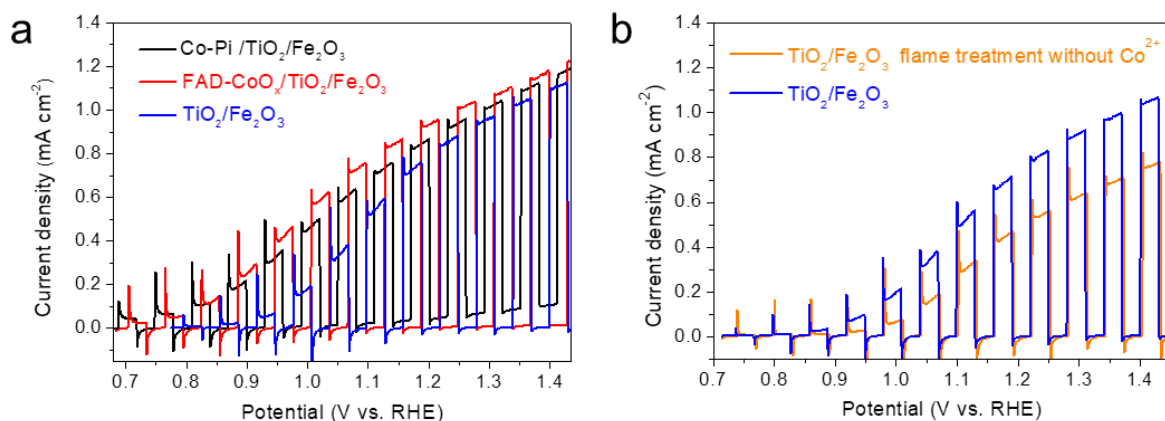


Figure S13. (a) Chopped irradiation curves of TiO₂/Fe₂O₃, Co-Pi/TiO₂/Fe₂O₃ and FAD-CoO_x/TiO₂/Fe₂O₃ photoelectrodes. (b) TiO₂/Fe₂O₃ photoanode with only methanol flame treatment without Co²⁺ for 1 min measured in 1.0 M KOH.

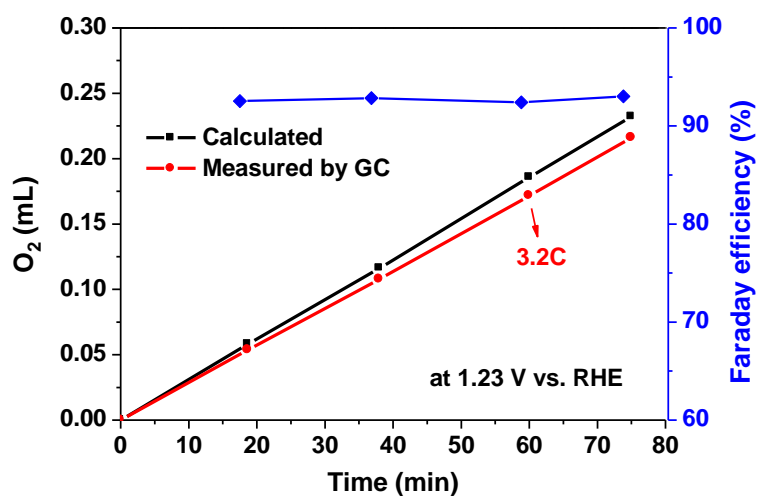


Figure S14. Faradic efficiency of FAD-CoO_x/TiO₂/Fe₂O₃ for light-driven water oxidation in 1.0 M KOH at an applied potential of 1.23 V vs. RHE. The Faradic efficiency was calculated from practical and theoretical oxygen evolution.

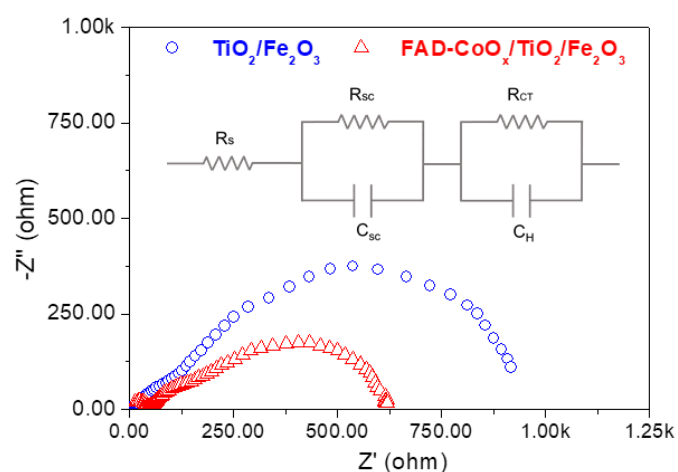


Figure S15. Nyquist plots of EIS measurements for $\text{TiO}_2/\text{Fe}_2\text{O}_3$ (blue) and $\text{FAD-CoO}_x/\text{TiO}_2/\text{Fe}_2\text{O}_3$ (red) measured at 0.9 V vs. RHE with AM 1.5G (100 mW cm^{-2}) in 1.0 M KOH. Inset: the equivalent circuit model.

Table S2. The values of fitting parameters for EIS tests

| | R_s (Ω) | R_{sc} (Ω) | R_{ct} (Ω) | $C_{sc} \times 10^{-4}$ (F) | $C_h \times 10^{-4}$ (F) |
|---|--------------------|-----------------------|-----------------------|-----------------------------|--------------------------|
| $\text{TiO}_2/\text{Fe}_2\text{O}_3$ | 21.29 | 101.9 | 853 | 1.052 | 2.81 |
| $\text{CoO}_x/\text{TiO}_2/\text{Fe}_2\text{O}_3$ | 20.05 | 119 | 446 | 1.038 | 3.2 |

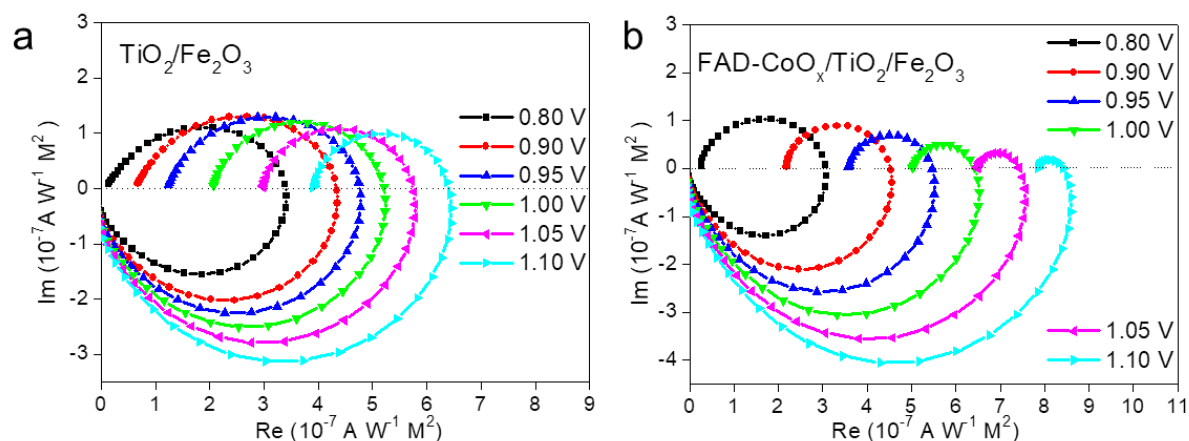


Figure S16. IMPS spectra of (a) $\text{TiO}_2/\text{Fe}_2\text{O}_3$ and (b) $\text{FAD-CoO}_x/\text{TiO}_2/\text{Fe}_2\text{O}_3$ photoelectrodes at different applied potentials.

Reference

- (1) Surendranath, Y.; Kanan, M. W.; Nocera, D. G. *J. Am. Chem. Soc.* **2010**, *132*, 16501.
- (2) Yang, Y.; Forster, M.; Ling, Y.; Wang, G.; Zhai, T.; Tong, Y.; Cowan, A. J.; Li, Y. *Angew Chem Int Ed Engl* **2016**, *55*, 3403.
- (3) Ahmed, M. G.; Kretschmer, I. E.; Kandiel, T. A.; Ahmed, A. Y.; Rashwan, F. A.; Bahnemann, D. W. *ACS Applied Materials & Interfaces* **2015**, *7*, 24053.
- (4) Zhong, D. K.; Sun, J.; Inumaru, H.; Gamelin, D. R. *Journal of the American Chemical Society* **2009**, *131*, 6086.
- (5) Daniel, Q.; Ambre, R. B.; Zhang, B.; Philippe, B.; Chen, H.; Li, F.; Fan, K.; Ahmadi, S.; Rensmo, H.; Sun, L. *ACS Catalysis* **2017**, *7*, 1143.
- (6) Bard, A. J. F., L. R. *Electrochemical methods: fundamentals and applications*; Wiley New York: Wiley New York.
- (7) Wu, Y.; Chen, M.; Han, Y.; Luo, H.; Su, X.; Zhang, M.-T.; Lin, X.; Sun, J.; Wang, L.; Deng, L.; Zhang, W.; Cao, R. *Angew. Chem. Int. Ed.* **2015**, *54*, 4870.
- (8) Zaharieva, I.; Chernev, P.; Risch, M.; Klingan, K.; Kohlhoff, M.; Fischer, A.; Dau, H. *Energy Environ. Sci.* **2012**, *5*, 7081.
- (9) Kanan, M. W.; Nocera, D. G. *Science* **2008**, *321*, 1072.
- (10) Gerken, J. B.; McAlpin, J. G.; Chen, J. Y. C.; Rigsby, M. L.; Casey, W. H.; Britt, R. D.; Stahl, S. S. *J. Am. Chem. Soc.* **2011**, *133*, 14431.
- (11) Jin, K.; Park, J.; Lee, J.; Yang, K. D.; Pradhan, G. K.; Sim, U.; Jeong, D.; Jang, H. L.; Park, S.; Kim, D.; Sung, N.-E.; Kim, S. H.; Han, S.; Nam, K. T. *J. Am. Chem. Soc.* **2014**, *136*, 7435.
- (12) Park, J.; Kim, H.; Jin, K.; Lee, B. J.; Park, Y.-S.; Kim, H.; Park, I.; Yang, K. D.; Jeong, H.-Y.; Kim, J.; Hong, K. T.; Jang, H. W.; Kang, K.; Nam, K. T. *J. Am. Chem. Soc.* **2014**, *136*, 4201.
- (13) Singh, A.; Chang, S. L. Y.; Hocking, R. K.; Bach, U.; Spiccia, L. *Energy Environ. Sci.* **2013**, *6*, 579.
- (14) Yu, F.; Li, F.; Zhang, B.; Li, H.; Sun, L. *ACS Catal.* **2015**, *5*, 627.